OPTIMAL TRAJECTORY PLANNING OF FORMATION FLYING SPACECRAFT

Dan Dumitriu [*,1] **Pedro U. Lima** [*] **Bogdan Udrea** [**]

[*] *Institute for Systems and Robotics*
Instituto Superior Técnico, Lisbon, Portugal
[**] *ESA/ESTEC, Noordwijk, Netherlands*

Abstract: This paper introduces a closed-loop Guidance and Control optimal algorithm that balances the propellant consumption and the need for collision avoidance among formation flying spacecraft. This model-based algorithm is purely algebraic and computes the spacecraft trajectories from the knowledge of the formation linearized relative dynamics equations and the formation full state. Using Pontryagin's maximum principle, Guidance generates the control inputs required to obtain the optimal trajectory from the current state until the target state, and does so for each of a set of regularly spaced time instants. After each recomputation, Control applies the optimal inputs until the next regularly spaced time instant, when Guidance updates the optimal trajectory again. Simulation results for the algorithm applied to a 3-spacecraft formation in GTO are presented.

Keywords: Satellite control, Trajectory planning, Optimal control, Obstacle avoidance

1. INTRODUCTION

A current and/or future trend in space science missions is the usage of several spacecraft flying in formation, in order to achieve higher accuracy in Earth and extra solar planetary observations or higher region coverage when monitoring science data, than what would be possible by using monolithic platforms. For example, to perform ground observation at very high spatial resolution of about 1 meter in the visible spectral band with a monolithic-mirror telescope, an aperture of about 30 meter would be required. However, such a monolithic-mirror telescope would have a much larger mass and would require the availability of a larger volume to be accommodated inside the launcher than a multi-spacecraft solution, e.g., based on interferometry. This interest reflects both in the European and American space programs, through ESA (e.g., DARWIN, LISA) and NASA (e.g., Earth Observing-1, Origins' NGST and TPF) planned or ongoing missions.

This paper concerns the guidance and control of a 3-spacecraft formation flying in Geostationary Transfer Orbit (GTO). More precisely, it concerns the guidance and control during the Formation Acquisition Maneuver (FAM), starting at time t_1 and ending at t_2. The guidance goal during FAM is to bring the 3 spacecraft from an initial randomly dispersed disposition at t_1 within a large sphere, to the desired final disposition at t_2, which is a tight formation. This must be performed while minimizing the propellant consumption of all spacecraft and avoiding collisions. In this work,

[1] The work of the first author has been supported by a grant of the ESA project "Formation Estimation Methodologies for Distributed Spacecraft", ESA contract No 17529/03/NL/LvH/bj

guidance means model-based trajectory planning, where the control inputs that lead to the desired trajectory are generated.

In related work (Campbell *et al.*, 2004), a generalized planning and control methodology for satellite formations, based on Hamiltonian-Jacobi-Bellman optimality, is presented. Fuel or time are minimized, but the control is based only on a bang-off-bang solution, and collision avoidance is not included in the cost function. In (Tillerson, 2002), linear programming is used to plan the optimal trajectories, by considering the linearized version of the relative dynamics equations in an eccentric orbit. Based on the same linearized dynamics, our algorithm plans the optimal trajectory using Pontryagin's maximum principle. The control solutions are continuous and collision avoidance is included in the cost function.

2. FORMATION FLYING DYNAMICS

2.1 Reference frames

The following 2 reference frames are considered:

(1) The *Inertial Planet Frame (IPQ)* is the reference inertial coordinate system, defined by:
- Origin: Earth mass center;
- $+\overrightarrow{x}_{IPQ}$ axis: in the equator plane, parallel to the Earth vernal equinox direction;
- $+\overrightarrow{y}_{IPQ}$ axis: completes the frame;
- $+\overrightarrow{z}_{IPQ}$ axis: from the Earth mass center towards North.

(2) The *Local Vertical Local Horizon* frame (*LVLH*, see Fig. 1) is used to locate the 3 spacecraft with respect to the reference orbit:
- Origin: located on the reference orbit;
- $+\overrightarrow{x}_{LVLH}$: completes the right-hand frame;
- $+\overrightarrow{y}_{LVLH}$: is normal to the orbital plane, opposite the angular momentum vector of the reference orbit;
- $+\overrightarrow{z}_{LVLH}$: points in the nadir direction.

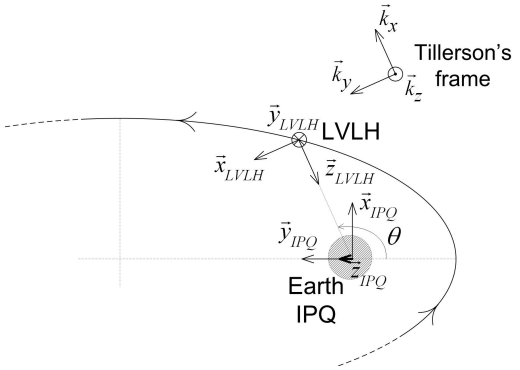

Fig. 1. LVLH, view from above the orbital plane

Remark 1. The origin of LVLH can be regarded as a virtual spacecraft placed on the reference orbit, **and** experiencing the same perturbations as the real ones. This virtual spacecraft located at LVLH's origin will be denoted by VSC_4.

One can obtain the transformation matrix $\mathbf{R}$ between IPQ and LVLH frames using the orbital parameters right ascension of the ascending node Ω, inclination i, argument of perigee ω and true anomaly θ (Sidi, 1997, p.24-26):

$$\mathbf{R} = [\mathbf{R}_z(\omega+\theta)\mathbf{R}_x(i)\mathbf{R}_z(\Omega)] \begin{bmatrix} 0 & 0 & -1 \\ 1 & 0 & 0 \\ 0 & -1 & 0 \end{bmatrix}$$

The following equivalent identities describe the transformations between representations of a position vector $\overrightarrow{x}$ in IPQ and LVLH:

$$\overrightarrow{x}_{IPQ} = \mathbf{R}\overrightarrow{x}_{LVLH} \Leftrightarrow \overrightarrow{x}_{LVLH} = \mathbf{R}^T\overrightarrow{x}_{IPQ}$$

where $\mathbf{R}^T$ denotes the transpose of matrix $\mathbf{R}$. For velocity vectors, the transformation is defined by:

$$\dot{\overrightarrow{x}}_{IPQ} = \dot{\mathbf{R}}\overrightarrow{x}_{LVLH} + \mathbf{R}\dot{\overrightarrow{x}}_{LVLH}$$

2.2 Relative Dynamics for Eccentric Orbits

The last two orbital parameters are the semi-major axis a and the eccentricity e. The natural frequency n of the reference orbit is defined by:

$$n = \sqrt{\frac{\mu}{a^3}} \quad \text{where } \mu = G{\cdot}m_{Earth} = 3.986{\cdot}10^5 \frac{\text{km}^3}{\text{s}^2}.$$

The orbit's true anomaly θ increases monotonically with time t and provides a natural basis for parameterizing the spacecraft motion. Thus, the differential dynamics equations will be expressed with respect to θ, rather than to t. For elliptic orbits, the relation between t and θ is (Sidi, 1997):

$$t - t_p = \frac{1}{n}\left[2\arctan\left(\sqrt{\frac{1-e}{1+e}}\tan\frac{\theta}{2}\right) - \frac{e\sqrt{1-e^2}\sin\theta}{1+e\cos\theta}\right] \tag{1}$$

where t_p is the passage time at the perigee.

The motion of each spacecraft in the formation is described with respect to the virtual spacecraft VSC_4, located in LVLH's origin. There are 3 spacecraft in the formation and subscript $i = 1, 2, 3$ will designate each of them. In the LVLH frame, the set of linearized θ-varying equations which describes the relative motion of the i^{th} spacecraft (denoted SC_i) in an eccentric orbit is ((Inalhan *et al.*, 2002), (Tillerson, 2002)):

$$\frac{d}{d\theta}\begin{bmatrix} x_i \\ x_i' \\ z_i \\ z_i' \end{bmatrix} = \mathbf{A}_{xz}(\theta)\begin{bmatrix} x_i \\ x_i' \\ z_i \\ z_i' \end{bmatrix} + \frac{(1-e^2)^3}{(1+e\cos\theta)^4 n^2}\begin{bmatrix} 0 & 0 \\ 1 & 0 \\ 0 & 0 \\ 0 & 1 \end{bmatrix}\begin{bmatrix} f_{x,i} \\ f_{z,i} \end{bmatrix} \tag{2}$$

$$\frac{d}{d\theta}\begin{bmatrix} y_i \\ y_i' \end{bmatrix} = \mathbf{A}_y(\theta)\begin{bmatrix} y_i \\ y_i' \end{bmatrix} + \frac{(1-e^2)^3}{(1+e\cos\theta)^4 n^2}\begin{bmatrix} 0 \\ 1 \end{bmatrix} f_{y,i} \tag{3}$$

where $\mathbf{A}_{xz}(\theta)$ is the following 4×4 matrix:

$$\mathbf{A}_{xz} = \begin{bmatrix} 0 & 1 & 0 & 0 \\ \frac{e\cos\theta}{1+e\cos\theta} & \frac{2e\sin\theta}{1+e\cos\theta} & \frac{-2e\sin\theta}{1+e\cos\theta} & 2 \\ 0 & 0 & 0 & 1 \\ \frac{2e\sin\theta}{1+e\cos\theta} & -2 & \frac{3+e\cos\theta}{1+e\cos\theta} & \frac{2e\sin\theta}{1+e\cos\theta} \end{bmatrix} \quad (4)$$

and $\mathbf{A}_y(\theta)$ is the following 2×2 matrix:

$$\mathbf{A}_y(\theta) = \begin{bmatrix} 0 & 1 \\ \frac{-1}{1+e\cos\theta} & \frac{2e\sin\theta}{1+e\cos\theta} \end{bmatrix} \quad (5)$$

Matrices $\mathbf{A}_{xz}(\theta)$ and $\mathbf{A}_y(\theta)$ depend only on θ.

x_i, y_i and z_i are the coordinates in LVLH frame of the relative position vector $\overrightarrow{\rho_i}$ of SC_i $(i = 1, 2, 3)$ with respect to VSC_4:

$$\overrightarrow{\rho_i} = \begin{bmatrix} x_i & y_i & z_i \end{bmatrix}^T \quad (6)$$

x_i' denotes $\frac{dx_i}{d\theta}$, $y_i' = \frac{dy_i}{d\theta}$ and $z_i' = \frac{dz_i}{d\theta}$. The relative positions x_i, y_i and z_i and the relative velocities x_i', y_i' and z_i' characterize the state of SC_i with respect to VSC_4. The relative dynamics equations (2) describe the in-plane motion, while equations (3) describe the out-of-plane motion.

$f_{x,i}$, $f_{y,i}$ and $f_{z,i}$ are the components in LVLH of the external forces vector $\overrightarrow{f_i}$, which includes the control inputs $\overrightarrow{u_i}$ acting on SC_i and the differential perturbations experienced by SC_i:

$$\overrightarrow{f_i} = \overrightarrow{u_i} + \sum \overrightarrow{w}_i$$

The differential perturbations are the relative perturbations experienced by SC_i with respect to the perturbations affecting VSC_4. There are several perturbations: J_2 effect, third-body (Sun, Moon) gravitational perturbations, solar radiation pressure, atmospheric drag, micrometeoroids.

In this paper, the closed-loop GC (guidance and control) algorithm neglects the differential perturbations, i.e., $\sum \overrightarrow{w}_i = 0$, since, along the trajectory arc where the maneuver is performed, they are small for the considered relative distances. However, when testing the algorithm in a realistic orbit dynamics simulator, all these perturbations are present. To take the unmodelled perturbations into account, as well as the state estimation errors, the closed-loop GC algorithm is recomputed periodically, and the planned trajectory is updated.

3. MODEL-BASED OPTIMAL TRAJECTORY PLANNING PROBLEM

During the Formation Acquisition Maneuver (FAM), i.e., between θ_1 and θ_2, with θ_1=$\theta(t_1)$ and θ_2=$\theta(t_2)$ as provided by (1), the trajectory of each spacecraft must minimize the propellant consumption and avoid collisions. The optimal trajectory planning problem during FAM includes:

- the state equations;
- the initial and final conditions;
- the limitations concerning the control inputs;
- the cost function to be minimized.

3.1 State equations

The state equations gather the relative dynamics equations of all 3 spacecraft. The global state variables vector is:

$$\mathbf{X} = \big[\, x_1 \;\; x_1' \;\; z_1 \;\; z_1' \;\; y_1 \;\; y_1' \;\; x_2 \;\; x_2' \;\; z_2 \;\; z_2' \;\; y_2 \;\; y_2' \;\; x_3 \;\; x_3' \;\; z_3 \;\; z_3' \;\; y_3 \;\; y_3' \,\big]^T$$

or, written by components:

$$X_1 = x_1,\ X_2 = x_1',\ X_3 = z_1,\ \ldots,\ X_{18} = y_3'$$

All control inputs are gathered into vector $\mathbf{U}$:

$$\mathbf{U} = \begin{bmatrix} u_{1,x} & u_{1,z} & u_{1,y} & u_{2,x} & u_{2,z} & u_{2,y} & u_{3,x} & u_{3,z} & u_{3,y} \end{bmatrix}^T$$

By putting together the linearized θ-varying relative dynamics equations (2) and (3) for all 3 spacecraft, the state equations of the model-based optimal trajectory planning problem are:

$$\frac{d\mathbf{X}}{d\theta} = \mathbf{A}(\theta)\mathbf{X} + \mathbf{B}(\theta)\mathbf{U} = \mathbf{f}(\mathbf{X}, \mathbf{U}, \theta) \quad (7)$$

where:

$$\mathbf{A}(\theta) = \begin{bmatrix} \mathbf{A}_{xz} & \mathbf{0}_{4\times2} & \mathbf{0}_{4\times4} & \mathbf{0}_{4\times2} & \mathbf{0}_{4\times4} & \mathbf{0}_{4\times2} \\ \mathbf{0}_{2\times4} & \mathbf{A}_y & \mathbf{0}_{2\times4} & \mathbf{0}_{2\times2} & \mathbf{0}_{2\times4} & \mathbf{0}_{2\times2} \\ \mathbf{0}_{4\times4} & \mathbf{0}_{4\times2} & \mathbf{A}_{xz} & \mathbf{0}_{4\times2} & \mathbf{0}_{4\times4} & \mathbf{0}_{4\times2} \\ \mathbf{0}_{2\times4} & \mathbf{0}_{2\times2} & \mathbf{0}_{2\times4} & \mathbf{A}_y & \mathbf{0}_{2\times4} & \mathbf{0}_{2\times2} \\ \mathbf{0}_{4\times4} & \mathbf{0}_{4\times2} & \mathbf{0}_{4\times4} & \mathbf{0}_{4\times2} & \mathbf{A}_{xz} & \mathbf{0}_{4\times2} \\ \mathbf{0}_{2\times4} & \mathbf{0}_{2\times2} & \mathbf{0}_{2\times4} & \mathbf{0}_{2\times2} & \mathbf{0}_{2\times4} & \mathbf{A}_y \end{bmatrix}$$

with $\mathbf{A}_{xz}$ expressed by (4) and $\mathbf{A}_y$ by (5). From (2) and (3), it is obvious to express $\mathbf{B}(\theta)$.

3.2 Boundary conditions and control inputs limitations

The optimal trajectory planning problem is studied between θ_1 and θ_2. Both the initial and the final state are given (see Section 4 for an example):

$$\mathbf{X}(\theta_1) = \mathbf{a} \;\text{ and }\; \mathbf{X}(\theta_2) = \mathbf{b} \quad (8)$$

The control inputs must satisfy the following constraint inequalities:

$$u_{\min} \leq |U_j| \leq u_{\max}, \;\text{ for } j = 1, \ldots, 9 \quad (9)$$

3.3 Cost function

The cost function must minimize propellant consumption, while ensuring collision avoidance. The relative distance between SC_i and SC_j is:

$$\rho_{ij} = \left\|\overrightarrow{\rho_j} - \overrightarrow{\rho_i}\right\| = \sqrt{(x_j - x_i)^2 + (y_j - y_i)^2 + (z_j - z_i)^2}$$

where the relative position vector $\overrightarrow{\rho_i}$ is defined in (6). The cost function to be minimized is:

$$J = J_{energy} + J_{avoidance} = \int_{\theta_1}^{\theta_2} L\left(\mathbf{X}(\theta), \mathbf{U}(\theta), \theta\right) d\theta$$

$$= \int_{\theta_1}^{\theta_2} \sum_{j=1}^{9} U_j^2 d\theta + \int_{\theta_1}^{\theta_2} \left[\delta_{12}(\rho_{12} - \rho_{\min})^2 + \right.$$

$$\left. + \delta_{13}(\rho_{13} - \rho_{\min})^2 + \delta_{23}(\rho_{23} - \rho_{\min})^2\right] d\theta \quad (10)$$

where $L(\mathbf{X}, \mathbf{U}, \theta)$ is the weight function. The first part J_{energy} of the cost function ensures the minimization of the overall control inputs between θ_1 and θ_2. Since the control inputs are proportional to the propellant consumption, the propellant consumption is minimized. By minimizing $J_{avoidance}$ we ensure collision avoidance.

In the expression (10) of the cost function, δ_{12}, δ_{13} and δ_{23} are weighting coefficients given by:

$$\delta_{ij} = \begin{cases} 0 & \text{if } \rho_{ij} \geq \rho_{\min} \\ \delta^0 & \text{if } \rho_{ij} < \rho_{\min} \end{cases} \quad \text{for } (ij) = (12), (13), (23)$$

As δ_{ij} is null for $\rho_{ij} \geq \rho_{\min}$, this defines $\rho_{\min}$ as the relative distance between spacecraft at which the collision avoidance term $\int_{\theta_1}^{\theta_2} \delta_{ij}(\rho_{ij} - \rho_{\min})^2 d\theta$ starts being considered. This is done by setting $\delta_{ij} = \delta^0 \neq 0$, with δ^0 chosen in order to ensure a convenient balance between J_{energy} and $J_{avoidance}$.

3.4 Application of Pontryagin's Maximum Principle

The model-based optimal trajectory planning problem consists of determining, for $\theta_1 \leq \theta \leq \theta_2$, the optimal trajectory $\mathbf{X}^{opt}(\theta)$ and the associated optimal control inputs $\mathbf{U}^{opt}(\theta)$, which:

- respect the state equations (7);
- meet the two-boundary conditions (8);
- satisfy the control inputs limitations (9);
- minimize the cost function given by (10).

This model-based optimal trajectory planning problem is solved by using Pontryagin's Maximum Principle (PMP) (Bryson and Ho, 1975). This optimization principle introduces 18 co-state (adjoint) variables λ_i, one for each state equation: λ_i corresponds to state equation $\dfrac{dX_i}{d\theta} = f_i(\mathbf{X}, \mathbf{U}, \theta)$, for $i = 1, \ldots, 18$. These adjoint variables are regrouped into the co-state vector $\mathbf{\Lambda}$:

$$\mathbf{\Lambda} = \begin{bmatrix} \lambda_1 & \lambda_2 & \ldots & \lambda_6 & \lambda_7 & \ldots & \lambda_{12} & \lambda_{13} & \ldots & \lambda_{18} \end{bmatrix}^T$$

By introducing the Hamiltonian:

$$H(\mathbf{X}, \mathbf{U}, \theta) = L(\mathbf{X}, \mathbf{U}, \theta) + \mathbf{\Lambda}^T \mathbf{f}(\mathbf{X}, \mathbf{U}, \theta)$$

and by expressing the co-state equations as:

$$\frac{d\mathbf{\Lambda}}{d\theta} = -\left(\frac{\partial H}{\partial \mathbf{X}}\right)^T = -\left(\frac{\partial L}{\partial \mathbf{X}}\right)^T - \frac{\partial \mathbf{f}^T}{\partial \mathbf{X}} \mathbf{\Lambda}, \quad (11)$$

the PMP states that the control inputs which satisfy, for all $\theta_1 \leq \theta \leq \theta_2$, the stationarity conditions:

$$0 = \left(\frac{\partial H}{\partial \mathbf{U}}\right)^T = \left(\frac{\partial L}{\partial \mathbf{U}}\right)^T + \frac{\partial \mathbf{f}^T}{\partial \mathbf{U}} \mathbf{\Lambda} \quad (12)$$

are the optimal ones, the corresponding trajectory being optimal as well.

Under the PMP formulation, the stationarity conditions (12) provide us with the optimal control inputs U_j^{opt}, as functions of the adjoint variables:

$$0 = \frac{\partial L}{\partial u_{1,x}} + \sum_{k=1}^{18} \frac{\partial f_k}{\partial u_{1,x}} \lambda_k = 2u_{1,x} + \frac{(1-e^2)^3}{(1+e\cos\theta)^4 n^2} \lambda_2$$

$$\Rightarrow \quad U_1^{opt} = u_{1,x}^{opt} = -\frac{1}{2} \frac{(1-e^2)^3}{(1+e\cos\theta)^4 n^2} \lambda_2 \ ,$$

$$U_2^{opt} = u_{1,z}^{opt} = -\frac{1}{2} \frac{(1-e^2)^3}{(1+e\cos\theta)^4 n^2} \lambda_4 \ , \qquad (\ldots)$$

So, the linear relation between the optimal control inputs and the adjoint variables is:

$$U_j^{opt} = -\frac{1}{2} \frac{(1-e^2)^3}{(1+e\cos\theta)^4 n^2} \lambda_{2j}, \ \text{ for } j = 1, \ldots, 9 \quad (13)$$

By taking into account the stationarity conditions (13), the state equations (7) at θ_k become:

$$\left.\frac{d\mathbf{X}}{d\theta}\right|_{\theta_k} = \mathbf{A}(\theta_k)\mathbf{X}(\theta_k) + \mathbf{B}^{\Lambda}(\theta_k)\mathbf{\Lambda}(\theta_k) \quad (14)$$

where:

$$\mathbf{B}^{\Lambda} = -\frac{1}{2}\left[\frac{(1-e^2)^3}{(1+e\cos\theta)^4 n^2}\right]^2 \begin{bmatrix} \mathbf{I}^*_{6\times 6} & \mathbf{0}_{6\times 6} & \mathbf{0}_{6\times 6} \\ \mathbf{0}_{6\times 6} & \mathbf{I}^*_{6\times 6} & \mathbf{0}_{6\times 6} \\ \mathbf{0}_{6\times 6} & \mathbf{0}_{6\times 6} & \mathbf{I}^*_{6\times 6} \end{bmatrix}$$

with:

$$\mathbf{I}^*_{6\times 6} = \begin{bmatrix} 0 & 0 & 0 & 0 & 0 & 0 \\ 0 & 1 & 0 & 0 & 0 & 0 \\ 0 & 0 & 0 & 0 & 0 & 0 \\ 0 & 0 & 0 & 1 & 0 & 0 \\ 0 & 0 & 0 & 0 & 0 & 0 \\ 0 & 0 & 0 & 0 & 0 & 1 \end{bmatrix}$$

3.5 Closed-loop GC algorithm

The differential linear two-boundary equations system to be solved consists of the state equations

(14) and the co-state equations (11). Both initial and final state vectors are known (8): $\mathbf{X}(\theta_1)$=$\mathbf{a}$ and $\mathbf{X}(\theta_2)$=$\mathbf{b}$, but there is no boundary condition available for the adjoint variables. The differential linear two-boundary equations system is solved by using the purely algebraic algorithm derived below, called closed-loop GC algorithm.

By using the finite differences expression of the derivative $\left.\frac{d\mathbf{X}}{d\theta}\right|_{\theta_k}$ for a constant step $\delta\theta$ in the true anomaly, and the short notation k instead of θ_k, equation (14) becomes:

$$\mathbf{X}(k{+}1) = \left[(\delta\theta)\mathbf{A}(k) + \mathbf{I}_{18}\right]\mathbf{X}(k) + \left[(\delta\theta)\mathbf{B}^{\Lambda}(k)\right]\mathbf{\Lambda}(k)$$

where $\mathbf{I}_{18}$ is the identity 18×18 matrix. Finally, the recurrent expression of the state variables is:

$$\mathbf{X}(k{+}1) = \overline{\mathbf{A}}(k)\mathbf{X}(k) + \overline{\mathbf{B}}(k)\mathbf{\Lambda}(k) \qquad (15)$$

where $\overline{\mathbf{A}}(k) = (\delta\theta)\mathbf{A}(k) + \mathbf{I}_{18}$ and $\overline{\mathbf{B}}(k) = (\delta\theta)\mathbf{B}^{\Lambda}(k)$. Similarly, the differential co-state equations (11) of the form:

$$\left.\frac{d\mathbf{\Lambda}}{d\theta}\right|_{\theta_k} = \mathbf{C}(k)\mathbf{\Lambda}(k) + \mathbf{D}(k)$$

can be transformed in the following recurrent expression of the adjoint variables:

$$\mathbf{\Lambda}(k{+}1) = \overline{\mathbf{C}}(k)\mathbf{\Lambda}(k) + \overline{\mathbf{D}}(k) \qquad (16)$$

where $\overline{\mathbf{C}}(k) = \delta\theta\mathbf{C}(k) + \mathbf{I}_{18}$ and $\overline{\mathbf{D}}(k) = \delta\theta\mathbf{D}(k)$.

Based on the recurrent expressions (15) and (16), $\mathbf{X}(k{+}1)$ can be expressed directly as function of $\mathbf{X}(0)$ and $\mathbf{\Lambda}(0)$, the same for $\mathbf{\Lambda}(k{+}1)$:

$$\mathbf{X}(k{+}1) = \mathbf{P}(k)\mathbf{X}(0) + \mathbf{Q}(k)\mathbf{\Lambda}(0) + \mathbf{S}(k) \qquad (17)$$

$$\mathbf{\Lambda}(k{+}1) = \mathbf{N}(k)\mathbf{\Lambda}(0) + \mathbf{V}(k) \qquad (18)$$

where $\mathbf{P}(k)$, $\mathbf{Q}(k)$, $\mathbf{S}(k)$, $\mathbf{N}(k)$ and $\mathbf{V}(k)$ are given by the following recurrent sequence:

(1) $\mathbf{P}(0) = \overline{\mathbf{A}}(0)$, $\mathbf{Q}(0) = \overline{\mathbf{B}}(0)$, $\mathbf{S}(0) = \mathbf{0}_{18}$ (null vector), $\mathbf{N}(0) = \overline{\mathbf{C}}(0)$, $\mathbf{V}(0) = \overline{\mathbf{D}}(0)$

(2) FOR k=1 TO $n{-}1$

$$\begin{aligned}
&\mathbf{P}(k) = \overline{\mathbf{A}}(k)\mathbf{P}(k{-}1)\\
&\mathbf{Q}(k) = \overline{\mathbf{A}}(k)\mathbf{Q}(k{-}1) + \overline{\mathbf{B}}(k)\mathbf{N}(k{-}1)\\
&\mathbf{S}(k) = \overline{\mathbf{A}}(k)\mathbf{S}(k{-}1) + \overline{\mathbf{B}}(k)\mathbf{V}(k{-}1)\\
&\mathbf{N}(k) = \overline{\mathbf{C}}(k)\mathbf{N}(k{-}1)\\
&\mathbf{V}(k) = \overline{\mathbf{C}}(k)\mathbf{V}(k{-}1) + \overline{\mathbf{D}}(k)
\end{aligned}$$

The recurrent sequence above is nothing else than propagating dynamics between θ_1=$\theta_{k=0}$ and θ_2=$\theta_{k=n}$. The number of steps n is related to the true anomaly step $\delta\theta$ by: $\delta\theta$=$\frac{\theta_1-\theta_2}{n}$. So, the initial state $\widehat{\mathbf{X}}(\theta_1)$, provided by an a priori estimation loop, corresponds to $\mathbf{X}(0)$, while the desired final state $\mathbf{X}(\theta_2)$ is the same as $\mathbf{X}(n)$. In this case, the expression (17) written for $k = n{-}1$ becomes:

$$\mathbf{Q}(n{-}1)\mathbf{\Lambda}(0) = \mathbf{X}(\theta_2) - \mathbf{P}(n{-}1)\widehat{\mathbf{X}}(\theta_1) - \mathbf{S}(n{-}1) \qquad (19)$$

where $\mathbf{Q}(n{-}1)$, $\mathbf{P}(n{-}1)$ and $\mathbf{S}(n{-}1)$ are provided by the recurrent sequence presented above. Expression (19) is an algebraic system of 18 linear equations, with unknowns $\mathbf{\Lambda}(0)$, that is, the initial adjoint variables at θ_1. This linear algebraic system is easily solved by using the Gauss elimination method. By using (18), the knowledge of $\mathbf{\Lambda}(0)$ provides us with the knowledge of all $\mathbf{\Lambda}(\theta)$, for $\theta_1 \le \theta \le \theta_2$. Finally, by means of the stationarity conditions (13) of the PMP formulation, all optimal control inputs $\mathbf{U}^{opt}(\theta)$ are known. The optimal trajectories $\mathbf{X}^{opt}(\theta)$ are known as well, by considering expressions (17).

The control inputs limitations (9) are considered only a posteriori. The obtained control inputs $\mathbf{U}^{opt}(\theta)$ are just not allowed to exceed the limitations. For example, if control inputs' component $\mathbf{U}_j^{opt}(\theta) > u_{\max}$, then $\mathbf{U}_j^{opt}(\theta) = u_{\max}$ is imposed.

4. NUMERICAL EXAMPLE

The closed-loop GC algorithm was tested in a realistic orbit dynamics simulator, including the several perturbations listed in Section 2.2. The results presented below concern a GTO orbit characterized by the following orbital parameters:

$$a = 26624.1\,\text{km},\ e = 0.7304,\ \Omega = 0,\ i = 7^\circ,\ \omega = -\frac{\pi}{2}.$$

The duration of FAM is chosen to be 4 h, in order not to saturate the control inputs, which limitations are: $u_{\min} = 0.1\,\mu$N, $u_{\max} = 50$ mN. FAM is centered in duration around apogee, where perturbations are much less significant than close to perigee. More precisely, FAM starts at t_1= 14416.94 s and ends at t_2=28816.94 s. The passage time at perigee was considered as the time origin: t_p=0. By using the relation (1), the corresponding true anomalies are: θ_1=165.5566 ° and θ_2=194.4434 °.

The initial state $\mathbf{X}(\theta_1)$=$\mathbf{a}$ corresponds to a random disposition of the 3 spacecraft within a sphere of 8 km in diameter, with the origin of LVLH as its center. The velocities included in $\mathbf{X}(\theta_1)$ have random values between −0.1 and 0.1 m/ s. The desired final state $\mathbf{X}(\theta_2)$=$\mathbf{b}$ corresponds to a tight formation. The goal is to attain, up to 1 h before the next orbit's apogee, an isosceles triangle formation with the equal edges of 250 m and with a 120^o angle between them. In order to meet this goal mostly by natural motion, by using the periodicity conditions (Inalhan *et al.*, 2002) for the unforced linearized equations of motion, the required tight formation $\mathbf{X}(\theta_2)$=$\mathbf{b}$ at the end of FAM is obtained. Table 1 presents both $\mathbf{a}$ and $\mathbf{b}$, only for spacecraft i=2.

The closed-loop GC algorithm is recomputed at regularly spaced time instants (every 70 s during the last $\frac{1}{2}$ h of FAM, and every 400 s for the rest of FAM), and the planned optimal trajectory is

Table 1. Initial and final states, in LVLH

	$X(\theta_1) = a$	$X(\theta_2) = b$
$x_2[\,\mathrm{m}]$	2996.28	-242.10
$\dot{x}_2[\frac{\mathrm{m}}{\mathrm{s}}]$	-0.041224	0.000559
$z_2[\,\mathrm{m}]$	-866.78	62.35
$\dot{z}_2[\frac{\mathrm{m}}{\mathrm{s}}]$	-0.040108	0.012858
$y_2[\,\mathrm{m}]$	296.12	0.00
$\dot{y}_2[\frac{\mathrm{m}}{\mathrm{s}}]$	-0.040155	0.000155

updated. Fig.2 presents a projection in the x-y plane of the 3 spacecraft relative trajectories in IPQ, where the relative positions are with respect to VSC_4. Fig.3 presents the evolution of the distances between SC_1 and SC_2, as well as between SC_1 and SC_3. Close to the goal, the distance between SC_1 and SC_2 goes down to 50 m, then the collision avoidance consideration together with the natural motion moves away the two spacecraft to the desired final distance. Fig.4 shows the control inputs that have been applied on SC_2, expressed in IPQ. The "reactions" to micrometeoroids are visible. Also noticeable is that control inputs are more reactive when the goal approaches.

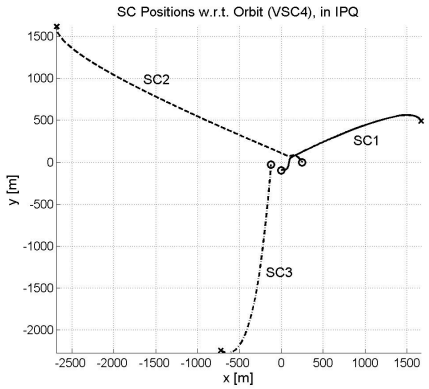

Fig. 2. Projection in the x-y plane of the 3 spacecraft relative trajectories in IPQ

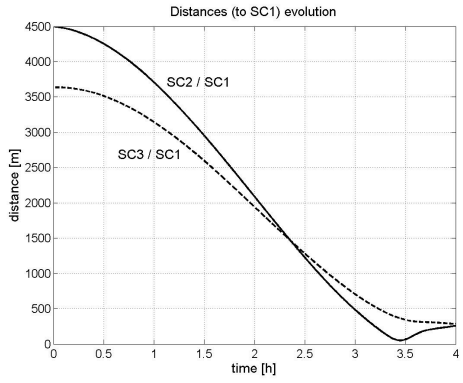

Fig. 3. The evolution of the distances between SC1 and SC2 (solid) and SC3 (dashed)

To conclude, the method of regularly recomputing the closed-loop GC algorithm successfully achieved an error between the obtained final state $\mathbf{X}(\theta_2)$ and the desired one $\mathbf{b}$ of the order of 0.1 m

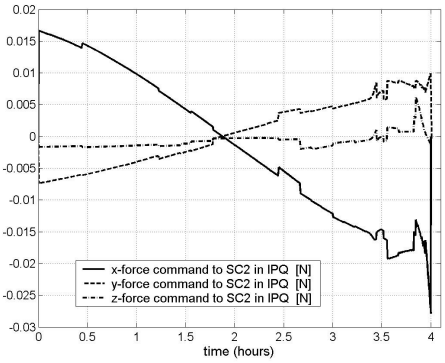

Fig. 4. SC2 optimal control inputs ($u_{2,x}$, $u_{2,y}$ and $u_{2,z}$) with respect to time t, in IPQ

for position components and of $0.05\frac{\mathrm{mm}}{\mathrm{s}}$ for velocities, which agrees with specifications for this mission.

5. CONCLUSIONS

This paper introduces a model-based optimal trajectory planning algorithm for formation flying spacecraft. This planning leads to trajectories that require less control effort during the trajectory tracking phase of the mission. This work is part of an ESA project where the formation state estimation is also handled by a decentralized estimator, and where the goal is to obtain simulation results for a 3-spacecraft formation flying in a GTO orbit with the estimator in the loop.

Acknowledgements

The authors would like to thank Augusto Caramagno, from DEIMOS Space, Luis Peñin and João Araújo from DEIMOS Engenharia, for useful insights on formation flying mission analysis and specification, as well as for making available DEIMOS' FF-FES simulator.

REFERENCES

Bryson, A.E. and Y.C. Ho (1975). *Applied optimal control.* Hemisphere Publishing Corporation. New York.

Campbell, M.E., D. Zanon and J. Kulkarni (2004). Cluster planning and control for spacecraft formations. *14th AAS/AIAA Space Flight Mechanics Conference.*

Inalhan, G., M.J. Tillerson and J.P. How (2002). Relative dynamics and control of spacecraft formations in eccentric orbits. *J. of Guidance, Control, and Dynamics* **25(1)**, 48–59.

Sidi, M.J. (1997). *Spacecraft Dynamics and Control - A Practical Engineering Approach.* Cambridge University Press.

Tillerson, M.J. (2002). *Coordination and Control of Multiple Spacecraft using Convex Optimization Techniques.* MSc report. Massachusetts Intitute of Technology.